Oluwajobi and Adebowale.: Nigerian Journal of Materials Science and Engineering.. Vol. 9:12-18 (2019)

The Finite Element Modelling of Selective Laser Melting of Metals

Oluwajobi A.O.* and **Adebowale** I.I.
Department of Mechanical Engineering, Obafemi Awolowo University, Ile-Ife, Osun State, Nigeria.

*Corresponding author: j.oluwajobi@gmail.com

Abstract
The Selective Laser Melting (SLM) is one of the Additive Manufacturing (AM) processes and it is more favoured over Selective Laser Sintering (SLS) because it can consolidate metal powders to a near full density (with relative density of more than 99%) and it can achieve a surface roughness of less than 20μm. However, the SLM process involves the use of high density energy laser to operate, by melting and re-solidification at very fast rates, which makes it very prone to defects and failures, like cracking, balling, delamination. Residual stresses are also caused by the high thermal gradient between the melt pool and the powder solid. A three-dimensional Finite Element Model (FEM) of selective laser melting was developed by using ANSYS software (workbench module 16.2) to predict the unsteady temperature evolution and distribution between the melt pool and the powder solid. The model incorporated a coupled thermal and mechanical simulation with convection. Temperature dependent material properties were also incorporated into the model. The moving heat source was described as a Gaussian distribution. It was observed that the heat accumulated during the previous scan tracks affected the next scan track and that the heat distribution to the surrounding powder bed was due to the fact that the heated-up material has greater conductivity than the untreated powder in front of the laser. This insight may be useful in the production of as-fabricated parts by the SLM process.

Keywords: Additive Manufacturing (AM), Selective Laser Melting (SLM), Finite Element Method (FEM)

1. INTRODUCTION
Additive manufacturing (AM) or 3-D printing is a term used to describe a range of digital manufacturing technologies, which produce component parts layer-by-layer through the additional use of materials. There are many different types of 3D printing processes, which are all controlled by using three-dimensional digital data. Some processes build parts by extruding molten plastic through a nozzle and depositing this accurately onto a build platform. Other technologies use lasers to melt layers of powdered material (like the Selective Laser Melting (SLM)), with other processes using ink-jet printing heads to deposit material into the shape of the desired component part.

As a 'tool-less' and digital approach to production, 3D printing has the potential to change the paradigm for manufacturing, away from mass production in centralized factories constrained by tooling and low-cost labour rates, to a world of mass personalization and distributed manufacturing. In this case, the choice of production location would be determined by the demographics of demand, rather than by the economics of supply.

AM by-passes many of the costly steps in conventional manufacturing; like getting equipment, acquiring the skills of metal working, and it allows solid free form designs to be transformed into near net-shaped metal objects, with the click of a key. Recent media attention and the advent of the 3D printing of a wide range of materials have created a hype and, in some cases, a false expectation, that in the near future any material will be rapidly printed into any size and shape. This is not yet the case and, in many instances, may never be, but the technology is moving in that direction. Large corporate investments are being made, in a very dynamic market both in the production of metal printing machines, in the demonstration and in the adoption of the technology (Chua and Leong, 2014).

The SLM-AM of metal use high density energy laser like the Nd-YAG fibre laser ($\lambda \approx 1.06$ μm), to scan powder metal selectively along the path, prescribed by the sliced data, from a CAD software, to build up part layer by layer. The process operates by melting and re-solidification at very fast rates, which makes it very prone to defects and failures like cracking, balling and delamination. Residual stresses are also caused by the high thermal gradient between the melt pool and the powder solid. These currently limit the use of SLM.

The AM of metals has its origins in a number of base or precursor technologies. Some of these have been around for 20 years, some for half a century or more. The advent of 3D printing with plastics and polymers created the rapid prototyping processes in wide use today and continue to serve as a precursor technology to AM metal printing. Stereolithography (SLA), was invented by Charles W. Hall in 1984 and it was commercialized by 3D Systems in 1989. The SLA

uses UV light to cure photopolymer into 3D shapes and the process is often cited as the origin of 3D printing. Fused Deposition Modeling (FDM) was developed in the late 1980s by S. Scott Crump and it was commercialized in 1990 by Stratasys. The FDM extrudes a thermoplastic through a heated nozzle to deposit planar layers into a 3D part (Kempen *et al.*, 2013).

In SLM, laser is irradiated onto a thin powder bed and the absorptivity of powder materials to laser irradiation can be drastically different from their corresponding bulk materials. Tolochko *et al.* (2007) investigated the absorptance of powder materials to infrared irradiation of CO_2 laser (wavelength, $\lambda \approx 10.6$ μm) and Nd-YAG laser ($\lambda \approx 1.06$ μm). In comparison to the absorptance of bulk materials with smooth surfaces, powder materials have significantly higher absorptance regardless of the wavelength of irradiation (Tolochko et al. 2007). For instance, at $\lambda \approx 1.06$μm, the absorptance of titanium bulk material is 30%, while that of titanium powder is 77%.

In an attempt to model the SLM process, Gusarov and Kruth (2010) compared the effective absorptance of powder bed with the absorptance of bulk material and match experimental data with both the isotropic specular reflection model and diffuse reflection model. The model, substantiated by the data, provides basis for prediction of the absorptance of powder bed based on that of bulk material. Their work provides models to calculate the ratio of the total absorption with respect to the material absorption and to predict the optimal laser parameters with which to process a particular material. The melt pool size in the SLM process was accurately predicted, by using the FEM (Foroozmehr *et al.*, 2016). They found out that the melt pool dimensions reached steady conditions in the third track. The FEM of SLM was also investigated by Bruna-Rosso el al. (2018). The reduced melt pool geometries were simulated in the first track, which led to lack of fusion defect formation. The SLM process is gaining a lot of attention because of its potential applications and so there is still need to study the process to be able to correctly predict the process parameters. In this paper, a finite element model of a moving heat source was developed to produce thermo-mechanical simulations of AM processes. This model can be used as a tool to predict the effect of process parameters in building parts using SLM, to reduce the amount of distortion and failures in the as-fabricated parts.

Figure 1 shows the SLM process parameters, which include the powder bed, the layer thickness, the hatching spacing, the substrate, the laser power and the direction of scanning speed. The nominal particle size

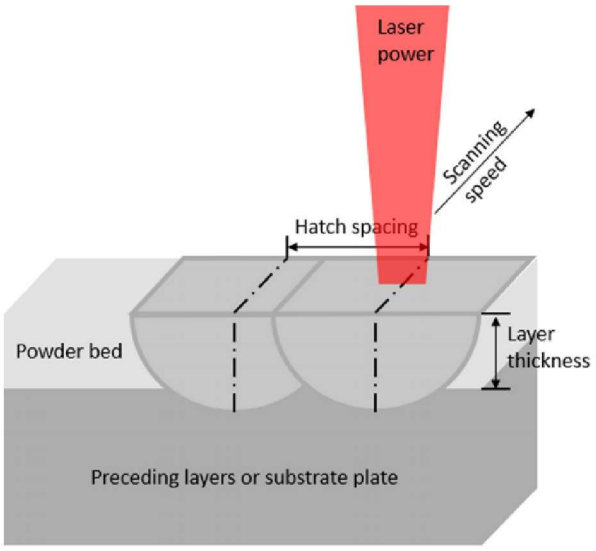

Figure 1: SLM Process Parameters (Yap *et al.*, 2015)

distribution of powder used in SLM is 10-45 μm.

The atmosphere under which metal is processed strongly affects the chemistry, the process ability and the heat transfer. Inert gas and/or vacuum systems are typically used, and each requirement leads to unique processing concerns.

The SLM-AM processes build on top of a metal substrate to achieve mechanical adherence of the first layers of the melted part. The substrate may be left at room temperature or heated by internal heaters. Most metal deposits form ductile interfaces and must be cut off the substrate during post-processing. The Ti6Al4V deposited on Stainless Steel 304 substrate forms a more brittle interface that can be removed by application of force, without cutting. This kind of interface is desirable for decreasing the number of post-processing steps (Hussein *et al.*, 2013).

Modelling of SLM

The process of SLM involves the moving of a laser beam across a powder bed to melt material layer by layer. From the standpoint of modeling, this simple procedure is complicated to capture accurately. The SLM involves very high laser intensity values, in the order of 10^{10} W/m^2 and a Heat Affected Zone (HAZ) that is the order of magnitude less than the dimensions of the platform. A complete and thorough understanding of temperature evolution is therefore fundamental to further improvements of the SLM process and fabricated products using this technology.

The FEM is identified as one of the most common methods of studying the temperature evolution and its melt pool. Several FEM models have been developed to study thermal distribution in SLM (Roberts *et al.*,

2009; Masoomi *et al.*, 2015; Huang *et al.*, 2016; Zhang *et al.*, 2018).

Governing Equation and Boundary Conditions

Heat energy is transferred and dissipated when a laser beam hits the powder bed surface in SLM: by conduction, convection and radiation. For a typical SLM machine such as EOS M270, fabrication takes place inside a closed build chamber purged using an inert gas like Argon. The heat transfer process can be described by a governing equation which follows the Fourier thermal principle (Equation 1):

$$\lambda(T)\nabla^2 T + q = \rho(T)c(T)\frac{\partial T}{\partial t} \quad \text{.....(1)}$$

The substrate is preheated to a certain temperature prior to fabrication (typically 353K in an EOS M270 machine). The prescribed temperature is described in Equation 2 as an initial condition of the problem.

$$T(x,y,z,0) = 0 \quad \text{..... (2)}$$

Heat convection occurs between the powder bed surface and the surrounding environment described by Equation 3.

$$-\lambda(T)\frac{\partial T}{\partial t}\bigg|_{z=H} = h(T - T_o) \quad \text{.....(3)}$$

Assuming no heat loss at the bottom surface of the substrate, a thermal boundary condition becomes (Equation 4):

$$T(x,y,0,t) = T_0 \quad (4)$$

Where T is the temperature, λ the conductivity coefficient, ρ the density, c the heat capacity coefficient, q the internal heat, T_0 the powder bed initial temperature, T_e the environment temperature, and h is the convective heat transfer coefficient.

The external heat flux q has been assumed to be a Gaussian heat flux (Equation 5):

$$q = \frac{2P}{\pi r_o^2}\exp-\left(\frac{2r^2}{r_o^2}\right) \quad \text{.....(5)}$$

Where P is the laser power, r_0 is the spot radius and r denotes the radial distance.

2. MATERIALS AND METHOD

In this study, a FE model was developed by using ANSYS Workbench 16.2, to determine the temperature evolution that occurs during the process of SLM. Equations 1 to 5 were employed in the model. The laser in this study is a continuous CO_2 laser (wavelength, λ≈10.6 μm) that is widely used in actual SLM process. At this wavelength, the absorption coefficient for Ti6Al4V powder was assumed to be 0.35.

Material Properties

The titanium alloy, Ti6Al4V powder, was used as the material for the simulation. The material properties of metals, for instance: the specific heat capacity, thermal conductivity, modulus of elasticity and yield stress, vary with temperature and these variations need to be considered during the simulation to get accurate results. Table 1 lists the various thermal and mechanical properties for Ti6Al4V.

The simulation was performed on a geometry that was developed in ANSYS Design Modeler, where a rectangular base was built with dimensions 2 mm (length) by 1 mm (width) by 0.1 mm (thickness). To define the prescribed path of the laser beam, a moving heat source was used which moved accordingly by the imprinted faces made on the rectangle 1 mm (length) by 0.4 mm (width) by 0.1 mm (thickness).

Table 1 : The Temperature-Dependent Properties of TI6AL4V

Temperature (°C)	Density (kg/m^3)	Specific Heat Capacity, Cp (J/K/kg)	Thermal Conductivity, k (W/m/K)	Coefficient of thermal expansion, α (μm/m/°C)	Modulus of Elasticity, E (GPa)	Yield Strength (MPa)	Poisson's Ratio
25	4430	565	6.60	8.60	104.00	768	0.34
93		565	7.30	8.70	101.00	735	
250		586	9.72	9.20	91.81	665	
500		682	13.92	9.70	78.63	552	
800		714	17.50	9.70	62.80	417	
1650		759	28.40	9.70	1.04	8	

Table 2: Model Properties Parameters.

Laser power	100W
Laser type	Gaussian distribution
Laser beam diameter	100µm
Scanning speed	250mm/s
Track length	1mm
Track number	4
Hatch space	100µm
Absorption rate	0.35

The simulation was performed on a geometry that was developed in ANSYS Design Modeler, where a rectangular base was built with dimensions 2.0 mm x 1.0 mm x 0.1 mm (length, width and thickness). To define the prescribed path of the laser beam, a moving heat source was used which moved accordingly by the imprinted faces made on the rectangle 1.0 mm x 0.4 mm x 0.1 mm.

The rectangular base has 0.1 mm as thickness to represent a 4-layer powder particle of 25 µm layer thickness. Then the geometry was imported to ANSYS mechanical where the 3D FEM model was meshed into 13790 elements (with 24403 nodes). One of the traditional scan patterns of the laser beam in SLM has been adapted for the model (See Figures 2-4).

The laser heat source acting on the top surface of Ti6Al4V powder bed was modeled as a mobile heat flux following Gaussian distribution along the axial axis with a constant speed. An initial temperature of 160°C was applied as a boundary condition to represent the preheated state at the beginning of the SLM process and the number of substeps for the analysis setting was 100 per steps.

All the external surfaces have a natural convection boundary condition of total heat transfer coefficient 80 $W/m^2/K$ with an external temperature of 160°C. The simulation generally required around 50 minutes of central processing unit (CPU) time on an Intel(R) Core(TM)i7-2670QM @2.2 GHz×2 (8GB RAM) laptop to obtain a solution.

3. RESULTS AND DISCUSSION

Figures 5-8 show the temperature profile that was predicted by the simulation at various times. The laser spot located at the start of the first track has a predicted temperature of powder layer as 2157.6°C under laser irradiation, exceeding the Ti6Al4V melting point of 1660°C to cause the occurrence of localized melting of powder. At around 0.3 mm (near to the beginning) the temperature increased to 2303.1°C and also increased further to 2326.5°C at around 0.6 mm (near the middle) due to low distribution of heat in the region under laser

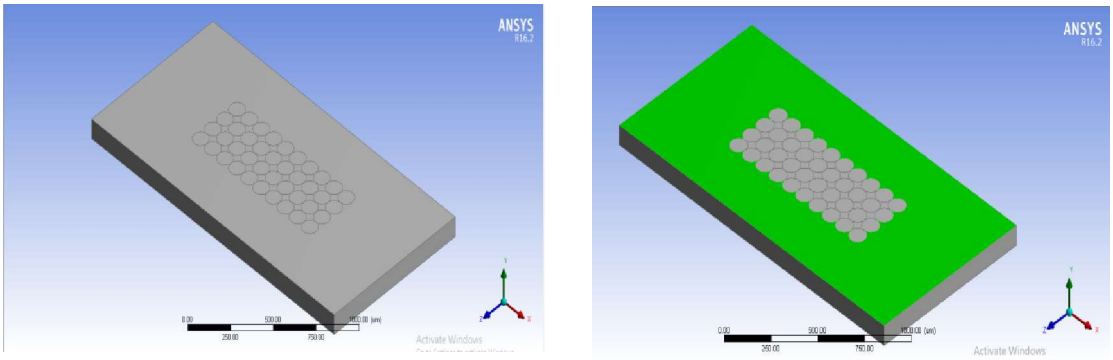

Figure 2: 3D Model of Rectangular Base of Ti6Al4V Powder

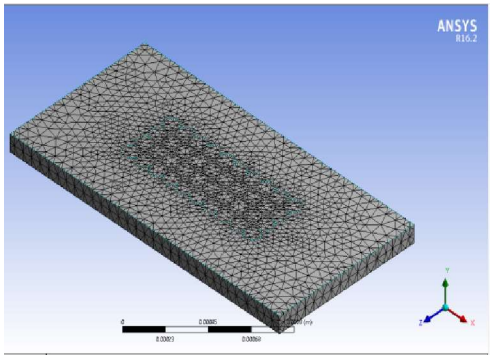

Figure 3: Dynamic Mesh of the Model

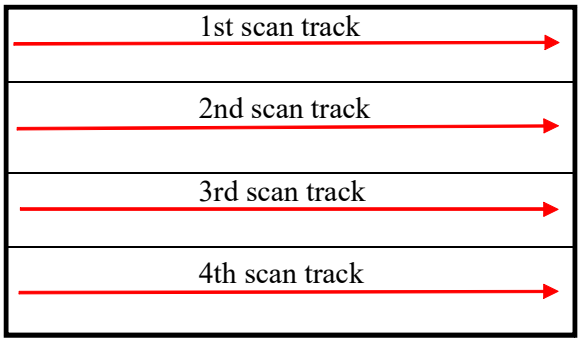

Figure 4: The Traditional Scan Pattern

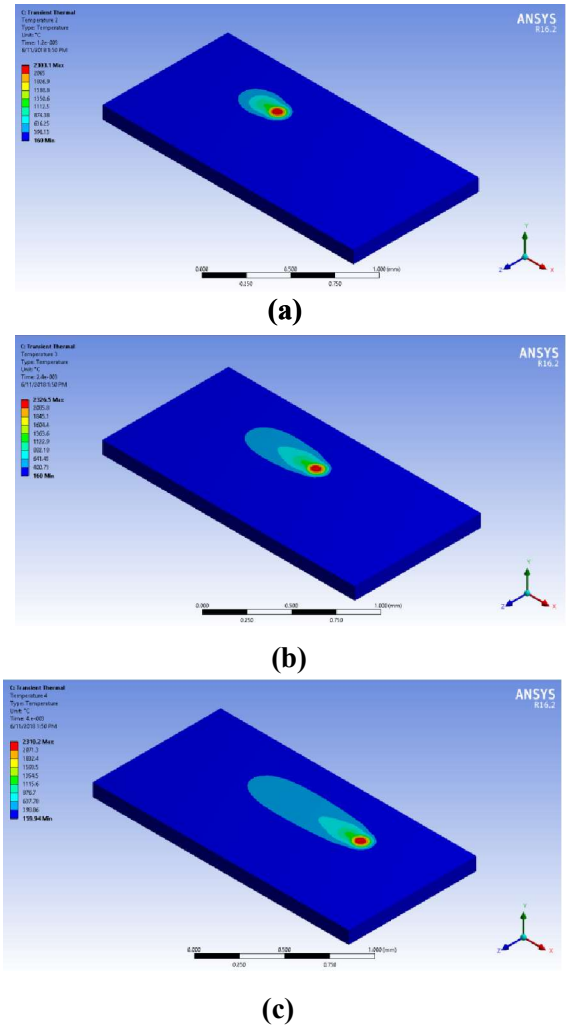

Figure 5: The predicted temperature evolution of the SLM model at the 1st track scan (a) Near to the beginning (b) Near the middle (c) The end.

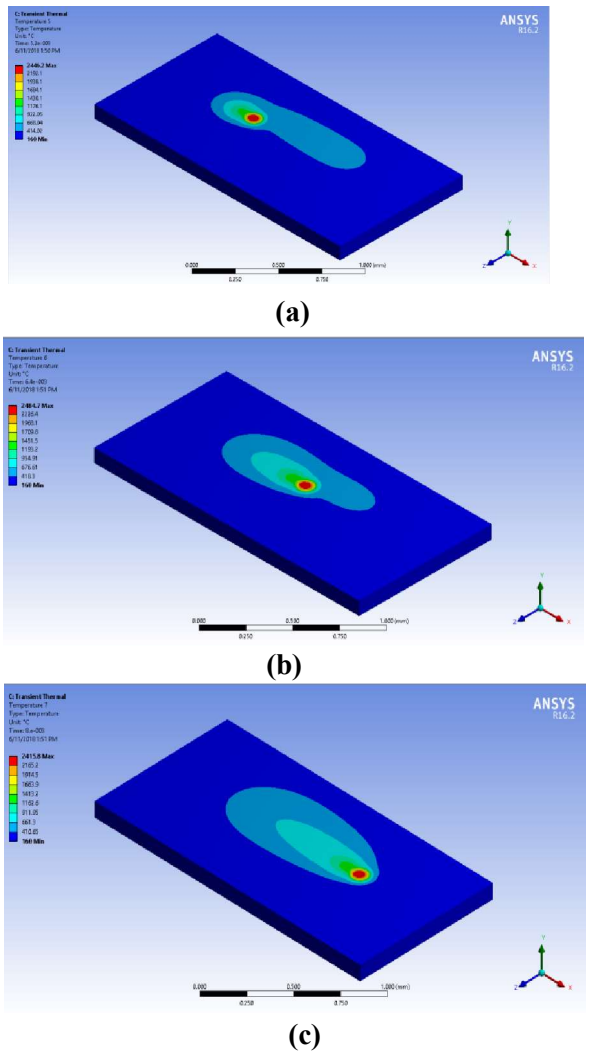

Figure 6: The predicted temperature evolution of the SLM model at the 2nd track scan (a) Near to the beginning (b) Near the middle (c) The end

irradiation. Nonetheless, this temperature dropped with increasing move distance of laser spot to 2310.2°C because of the heat distribution into the surrounding powder bed which caused a long "comet tail" profile which can be seen in Figure 5 (the end). This can also be attributed to the fact that the heated-up material has greater conductivity than the untreated powder in front of the laser.

At the beginning of the second track, the temperature increased to 2446.2°C which can be seen to be due to the heat accumulated during the first track at which the temperature profile appears to be merging together, which also further increased the temperature to 2484.7°C shown at the middle of the second track. The temperature can be seen to be reduced to 2415.8°C at the end of the second track due to enough time for the distribution of heat into the surrounding powder.

During, the third scan track, it can be seen that the temperature evolution followed the same pattern as that of the second track. By beginning with high temperature that is due to the heat accumulated during the previous track and further increased at the middle of the scan track and later reduced towards the end after enough time for heat distribution and the fact that the heated-up material has greater conductivity than the untreated powder in front of the laser. Figure 7 shows the temperature profile of the third track during the beginning, the middle and the end (2518.8°C, 2582.8°C and 2500.8°C respectively).

The fourth and the last scan also behaved in the same way as that of the previous scan tracks, as the laser spot further moved to the end of the fourth track, the temperature contour and profile are noted to be bigger and larger than the previous scan tracks. The combined results of greater heat accumulation and a longer interaction time of the laser beam with the powder bed

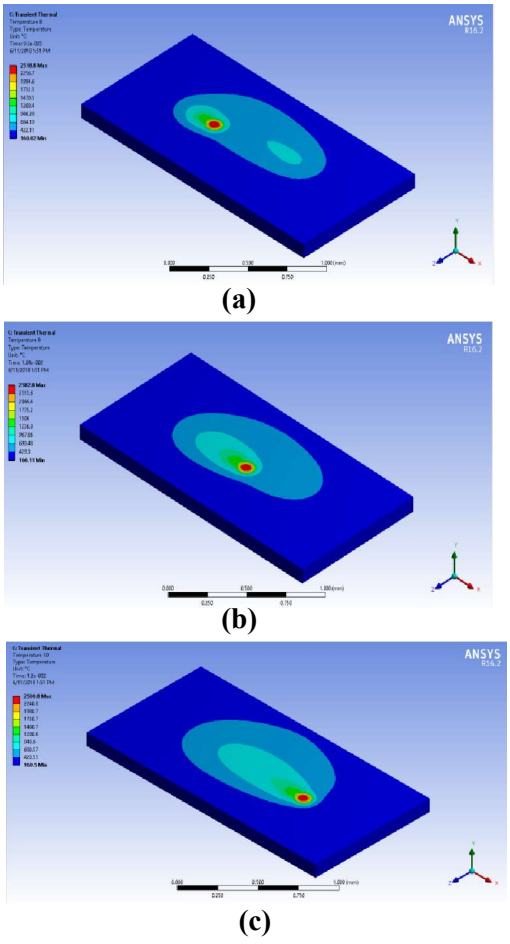

Figure 7: The predicted temperature evolution of the SLM model at the 3rd track scan (a) Near to the beginning (b) Near the middle (c) The end

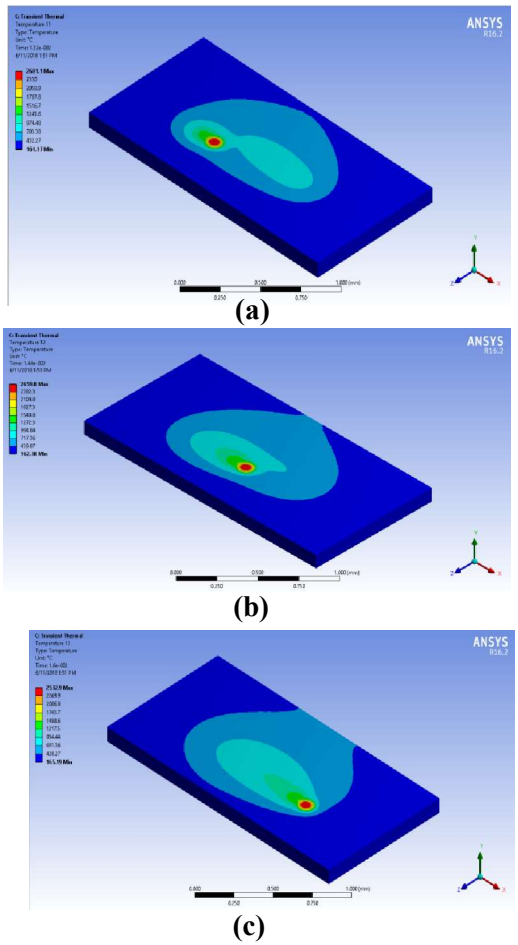

Figure 8: The predicted temperature evolution of the SLM model at the 4th track scan (a) Near to the beginning (b) Near the middle (c) The end

also produced a higher temperature at the end for the last track. The temperatures of the last track at the beginning, the middle and the end according to Figure 8 are 2601.1°C, 2659.8°C and 2532.9°C respectively.

It can be deduced from the predicted temperature profiles that the more the scan tracks, the more the heat accumulation which affected the next scan track and that the more time spent on a single scan track, the better the heat distribution to the surrounding powder bed due to the fact that the heated-up material has greater conductivity than the untreated powder in front of the laser.

After the simulation was performed, the results were compared with the work of Yee-Ting *et al* (2017). In that study, the finite element method (FEM) software ANSYS (work bench module 16.0) was used to predict the unsteady temperature distribution for resolving molten pool dimensions with consideration of temperature-dependent thermal physical properties of Ti-6Al-V4 at different laser powers and scanning speeds. The temperature distributions over time were

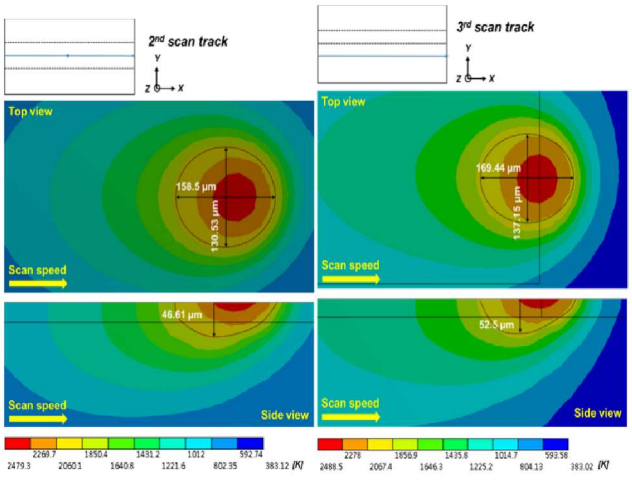

Figure 9: Time sequences of predicted temperature contours on the top surface of 3D melt pool at various locations including (a) the center of the second track and (b) the end of the third track for the laser power of 95 W and scanning speed of 210 mm/s during SLM of TiAl6V4 powder - Yee-Ting's model. (Yee-Ting *et al*., 2017).

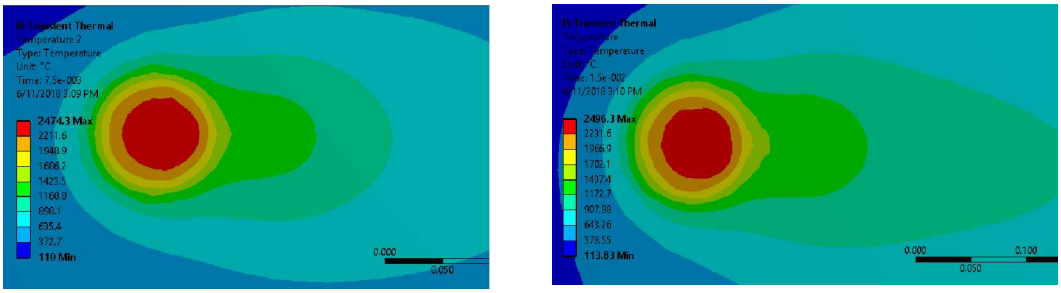

Figure 10: Time sequences of predicted temperature contours on the top surface of 3D melt pool at various locations including (a) the center of the second track and (b) the end of the third track for the laser power of 95 W and scanning speed of 210 mm/s during SLM of TiAl6V4 powder - current model.

compared with the results obtained by Yee-Ting. The laser scan area on a Ti-6Al-4V powder layer had a length of 3.0 mm, a width of 3.0 mm, and a depth of 0.03 mm. The dimensions of powder bed were 3.0 mm in length, 3.0 mm in width, and 1.0 mm in depth, respectively. The model used the processing parameters of: Laser power P, 95W; Scan speed, V, 210 mm/s; Laser spot radius, Ω, 0.05 mm; Track length, l, 0.85 mm; Powder layer thickness, δ, 0.03 mm; Track number, Nt, 3.

The temperature contours at different time intervals are given in Figures 9 and 10 for both the Yee-Ting's model and current model respectively. The temperature reached at the end of the 3rd scan track in the current model was 2496.3°C. This compares favourably with Yee-Ting *et al.* model of 2483.5°C.

4. CONCLUSION

Taking the mobile gaussian distribution of the heat flux and the temperature-dependent thermophysical parameters into consideration, a 3D FEM model was developed to investigate the temperature evolution during the SLM of Ti6Al4V powder. The laser beam moving from the start to the end of tracks led to unsteady temperature profiles during the process. This was mainly due to the heat accumulation effect and the temperature distribution through conduction, rather than through convection and radiation, during SLM.

The model can predict temperature evolution and the distribution of the part during the build. The optimal process parameters of laser beam power, laser beam speed and powder layer thickness can then be identified for a given shape or geometry.

5. REFERENCES

Bruna-Rosso C., Demir A.G. and Previtah R. (2018). Selective laser melting finite element modelling: validation with high-speed imaging and lack of fusion defects prediction, Materials and Design, 156: 143-153

Chua, C. K. and Leong, K. F. (2014). 3D printing and additive manufacturing: principles and applications, 4ed. World Scientific, Singapore.

Foroozmehr A., Badrossamay M., Foroozmehr E. and Golabi S. (2016). Finite element simulation of selective laser melting process considering optical penetration depth of laser in power bed, Materials and Design, 89: 255-263.

Gusarov, A. V., and Smurov, I. (2010). Modeling the interaction of laser radiation with powder bed at selective laser melting, Phys Procedia, 5: 381–394.

Huang, Y., Yang, L. J., Du, X. Z. and Yang, Y. P. (2016). Finite element analysis of thermal behavior of metal powder during selective laser melting, Int. J. Therm. Sci., 104: 146-157.

Hussein, A., Hao, L., Yan, C. and Everson, R.(2013). Finite element simulation of the temperature and stress fields in single layers built without-support in selective laser melting, Mater. Des., 52: 638–647.

Kempen, K., Vrancken, B., Thijs, L., Buls, S., Van Humbeeck, J. and Kruth, J. P. (2013), in *Solid Freeform Fabrication Symposium Proceedings,* 2013, Austin, TX, USA (The University of Texas at Austin).

Masoomi, M., Alaa, E., Shamsaei, N. and Thompson, S (2015). Modeling, simulation and experimental validation of heat transfer during selective laser melting," in *Proceedings of the ASME 2015 International Mechanical Engineering Congress & Exposition,* Houston.

Roberts, I. A., Wang, C. J., Esterlein, R., Stanford, M. and Mynors, D.J. (2009). A three-dimensional finite element analysis of the temperature field during laser melting of metal powders in additive layer manufacturing, Int. J. Mach. Tools Manuf., 49: 916–923.

Yap, C. Y., Chua, C. K., Dong, Z. L., Liu, Z. H., Zhang, D. Q., Loh, L. E. and Sing, S. L. (2015). Review of selective laser melting: Materials and applications, Applied Physics Reviews 2, 4: 041101

Yee-Ting Lee, Jyun-Rong Zhuang, Wen-Hsin Hsieh, An-Shik Yang, (2017). FEM simulations to study the effects of laser power and scan speed on molten pool size in additive manufacturing, International Journal of Mechanical and Mechatronics Engineering, 11,7: 1298-1302.

Zhang Y., Guillemot G., Bernacki M. and Bellet M. (2018). Macroscopic thermal finite element modelling of additive metal manufacturing by selective melting process, Computer Methods in Applied Mechanics and Engineering, 331: 514-535.